



## The structure of genetically modified iron–sulfur cluster $F_X$ in photosystem I as determined by X-ray absorption spectroscopy

Xiao-Min Gong<sup>a</sup>, Yehoshua Hochman<sup>a</sup>, Tal Lev<sup>a</sup>, Grant Bunker<sup>b</sup>, Chanoch Carmeli<sup>a,\*</sup>

<sup>a</sup> Department of Biochemistry, Tel Aviv University, Tel Aviv 69978, Israel

<sup>b</sup> Department of Physics, Illinois Institute of Technology, Chicago, ILL 60616-3793, USA

### ARTICLE INFO

#### Article history:

Received 28 June 2008

Received in revised form 5 November 2008

Accepted 11 November 2008

Available online 21 November 2008

#### Keywords:

Photosystem I

Photosynthesis

Iron–sulfur cluster

X-ray absorption

Electron transfer

Subunit deletion

Site directed mutation

Transient absorption spectroscopy

### ABSTRACT

Photosystem I (PS I) mediates light-induced electron transfer from P700 through a chlorophyll *a*, a quinone and a [4Fe–4S] iron–sulfur cluster  $F_X$ , located on the core subunits PsaA/B to iron–sulfur clusters  $F_{A/B}$  on subunit PsaC. Structure function relations in the native and in the mutant (*psaB*-C565S/D566E) of the cysteine ligand of  $F_X$  cluster were studied by X-ray absorption spectroscopy (EXAFS) and transient spectroscopy. The structure of  $F_X$  was determined in PS I lacking clusters  $F_{A/B}$  by interruption of the *psaC2* gene of PS I in the cyanobacterium *Synechocystis* sp PCC 6803. PsaC-deficient mutant cells assembled the core subunits of PS I which mediated electron transfer mostly to the phylloquinone. EXAFS analysis of the iron resolved a [4Fe–4S] cluster in the native PsaC-deficient PS I. Each iron had 4 sulfur and 3 iron atoms in the first and second shells with average Fe–S and Fe–Fe distances of 2.27 Å and 2.69 Å, respectively. In the C565S/D566E serine mutant, one of the irons of the cluster was ligated to three oxygen atoms with Fe–O distance of 1.81 Å. The possibility that the structural changes induced an increase in the reorganization energy that consequently decreased the rate of electron transfer from the phylloquinone to  $F_X$  is discussed.

© 2008 Elsevier B.V. All rights reserved.

### 1. Introduction

Photosystem I (PS I) is a multisubunit complex located in the thylakoid membranes of chloroplasts and cyanobacteria. It mediates light-induced electron transfer from plastocyanin or cytochrome  $C_{553}$  to ferredoxin [1,2]. In cyanobacteria, the complex consists of 12 polypeptides, some of which bind light-harvesting chlorophyll molecules. The reaction center core complex is made up of the heterodimeric PsaA and PsaB subunits, containing the primary electron donor P700, which transfers an electron through the sequential carriers  $A_0$ ,  $A_1$  and  $F_X$ . The final acceptors  $F_A$  and  $F_B$  are located on another subunit, PsaC. P700 is a chlorophyll *a* heterodimer, which undergoes light-induced charge separation. The electron carriers  $A_0$ ,  $A_1$ ,  $F_X$ ,  $F_A$  and  $F_B$  represent a monomeric chlorophyll *a*, a phylloquinone and three [4Fe–4S] iron sulfur centers, respectively. The crystal structure of PS I from *Thermosynechococcus elongatus* [3]

(*TS. elongatus*) and from plant [4] were resolved at 2.5 Å and 3.5 Å, respectively. In cyanobacteria each of the heterodimeric core subunits PsaA and PsaB of PS I contains 11 transmembranal helices.  $F_X$  is located in the center of the core heterodimer at the interface of subunit PsaC.  $F_X$  is bound at this interface to interhelical loops of both subunits PsaA and PsaB. The cysteine residues in the two subunits of the heterodimer, which are in an identical amino acid sequence CDGPGRGGTC [5], bind the iron–sulfur cluster. The two cysteines C556 and C565 in PsaB of *Synechocystis* sp PCC 6803, which are analogous to C565 and C574 in *TS. elongatus*, are the ligands of  $F_X$ . Thus  $F_X$  is positioned as an intermediate carrier between the initial electron mediators  $A_0$  and  $A_1$  and the final electron acceptors of PS I  $F_A$  and  $F_B$ .

The crystal structure determination of PS I placed  $F_X$  between  $A_1$  and  $F_A$  with edge to edge distance of 6.8 Å between  $A_1$  and  $F_X$ , and 10.1 Å between  $F_X$  and  $F_A$  [3]. The midpoint potential of  $F_X/F_X^+$  is about –700 mV [6], the lowest among the iron–sulfur clusters known in biology. It therefore has the properties required for a carrier that mediates electrons between  $A_1$ , with an estimated redox potential of –800 mV to –700 mV [7], and  $F_A$  with –530 mV [8]. Forward electron transfer was directly shown to proceed through  $F_X$  at room temperature by optical spectroscopy [9] and by EPR [10]. An approximate lifetime of 200 ns by EPR [10,11] and two components of 10–30 ns and about 200 ns by optical method [12–16] for the oxidation of  $A_1^-$  by  $F_X$  were determined. The presence of two kinetic components for the oxidation of  $A_1^-$  may reflect the use of two similar,

**Abbreviations:**  $A_0$ , primary electron acceptor in PS I;  $A_1$ , secondary electron acceptor in PS I; Chl, chlorophyll; DCIP, 2,6-dichlorophenolindophenol; LAHG, light-activated heterotrophic growth; P700, primary electron donor of PS I; PS I, photosystem I;  $F_X$ ,  $F_A$  and  $F_B$ , [4Fe–4S] clusters of PS I; XAS, X-ray absorption-spectroscopy; XANES, X-ray absorption-near edge structure; EXAFS, X-ray-extended fine structure

\* Corresponding author. Tel.: +972 3 6409826; fax: +972 3 6406834.

E-mail address: [ccarmeli@post.tau.ac.il](mailto:ccarmeli@post.tau.ac.il) (C. Carmeli).

<sup>1</sup> An abstract of an oral presentation in a conference of this work was published: Carmeli, C., et al. *Biochim. Biophys. Acta. Bioener.* 2006, 14, 263.

but not identical electron transfer branches in PS I [14,15], although other explanations are still under discussion [17]. Electron transport from  $A_1$  through  $F_X$  to  $F_A$  and  $F_B$  appears to be modulated by a variety of environmental factors (for review see [17]).

The structure of  $F_X$  was obtained by modeling a distorted cubane [4Fe–4S] cluster into the electron density obtained from the X-ray diffraction of the PS I crystals [3]. In this structure an average Fe–S and Fe–Fe distance of 2.28 Å and 2.72 Å, respectively, was determined. A similar structure was determined earlier by X-ray absorption fine structure analysis (EXAFS) of the iron in core subunits prepared by chemical dissociation of PS I from the cyanobacterium *Synechococcus* 6301 [18]. Although some of the PsaC subunit remained attached to the PsaA/B core subunits no EPR signal of  $F_{A/B}$  iron sulfur clusters could be detected in this preparation. The results were best fitted to a [4Fe–4S] cluster with Fe–S and Fe–Fe average distance of 2.27 Å and 2.70 Å, respectively. However, the structure of a modified  $F_X$  in which cysteine ligands of the cluster were altered by mutations has not been well resolved. Based on EPR measurements, the mutants of the cysteine ligands C556S and C565S in PsaB subunit of PS I were first suggested to be a mixture of [3Fe–4S] and [4Fe–4S] and later as a modified mixed ligand [4Fe–4S] cluster [19,20]. In this work we report the determination of the structure by EXAFS analysis of genetically modified  $F_X$ . The measurements were done in the core subunits prepared from PS I lacking subunit PsaC and therefore devoid of the associated  $F_{A/B}$  clusters. In order to avoid possible complication that might arise from residual PsaC attached to the core, the subunit was removed by interruption of the *psaC* gene in the cyanobacterium *Synechocystis* sp. PCC 6803 [16]. There was a substantial decrease in electron transport to  $F_X$  in the PsaC-depleted PS I, but this was not a result of depletion of the iron–sulfur cluster  $F_X$ . By quantification of acid-labile sulfide and iron, the lack of effect of  $F_X$  reconstitution treatment, the partial recovery of long-lived charge separation upon rebinding of the extrinsic subunits and reconstitution of  $F_A$  and  $F_B$ , we have shown [16] that  $F_X$  is present and potentially functional in the isolated PsaC-deficient PS I. The PsaC-depleted preparation was reconstituted by the addition of subunits PsaC, PsaD and PsaE in the presence of  $\beta$ -mercaptoethanol,  $Fe^{3+}$  and  $S^{2-}$  that regenerated the iron–sulfur clusters  $F_{A/B}$ . Indeed the presence of  $F_X$  is supported by structural determination of the cluster by EXAFS analyses as shown in this work. The measurements were done in the wild type and in PS I mutated in a cysteine ligand of  $F_X$  in PsaB. The findings offer for the first time a structural basis for understanding the function of the modified  $F_X$  in PS I.

## 2. Experimental procedures

### 2.1. Cyanobacterial strains and growth conditions

Glucose-tolerant *Synechocystis* sp. PCC 6803 cells were grown in BG-11 medium supplemented with 5 mM TES, pH 8.0, and 5 mM glucose at 30 °C [21]. Mixotrophic cultures were grown in continuous light at photon flux density of 40  $\mu\text{mol m}^{-2} \text{s}^{-1}$ . Heterotrophic cultures were grown in dim light (photon flux density of 2  $\mu\text{mol m}^{-2} \text{s}^{-1}$ ), or under light-adapted heterotrophic growth (LAHG) conditions: in complete darkness, except for 10 min of light (photon flux density of 40  $\mu\text{mol m}^{-2} \text{s}^{-1}$ ) every 24 h [22]. For photoautotrophic growth, cells were grown in the medium without glucose in continuous light (photon flux density of 40  $\mu\text{mol m}^{-2} \text{s}^{-1}$ ). Insertion inactivation of the *psaC2* gene in wild type and in mutant C565S/D566E in PsaB [23] were done as previously described [16]. PsaB and PsaC mutants were grown in medium supplemented with kanamycin (25  $\mu\text{g/ml}$ ) and spectinomycin (20  $\mu\text{g/ml}$ ), respectively, under heterotrophic growth conditions. For growth on plates, BG-11 medium was supplemented with 1.5% (w/v) bacto-agar and 0.3% sodium thiosulfate [24]. Growth of cells was monitored by measurement of absorption changes at 730 nm.

### 2.2. Isolation of thylakoid membranes and PS I complexes

Harvested cells were washed and broken in a French Pressure Cell at 500 psi and thylakoids were isolated. PS I was solubilized by the detergent *n*-dodecyl  $\beta$ -D-maltoside and purified on DEAE-cellulose columns and on a sucrose gradient as described [16].  $Na_2S$  (10 mM) was added to the isolation medium when indicated. SDS polyacrylamide gel electrophoresis (SDS-PAGE) and Western blotting were done as previously described [25,26]. Protein in the membranes was determined after solubilization in 1% SDS as described [27]. Chlorophyll concentration and P700 chemical- and photo-oxidation were determined as reported [28,29].

### 2.3. Spectroscopic measurements

The kinetics of P700<sup>+</sup> reduction were measured by monitoring flash-induced transient absorption changes at 700 nm. Measurements at 700 nm used a modified flash photolysis setup as described earlier [30] which included a 10 ns flash from Quantal Nd-YAG laser at 532 nm and energy of 1 mJ/cm<sup>2</sup>. A measuring beam was provided by a tungsten-iodide source passed through a monochromator. The absorption changes at 700 nm were monitored by a photomultiplier, interfaced by Tektronix TDS 520A Digitizing Oscilloscope, and recorded on a PC computer. Typically, several hundred transitions were averaged at a repetition rate of 1 Hz. Absorption change transients were analyzed by fitting with a multiexponential decay using Marquardt least-squares algorithm programs (KaleidaGraph 3.5 from Synergy Software, Reading, PA).

### 2.4. X-ray absorption (XAS)

#### 2.4.1. Sample preparation

For sample preparation PS I core preparation was precipitated by centrifugation from a solution containing 30% polyethylene glycol 6000, 50 mM NaCl, 20 mM Tricine–KOH, pH 8, 0.05%  $\beta$ -dodecyl maltoside and 20% sucrose. The pellet was loaded onto a window (10 mm  $\times$  2 mm  $\times$  0.5 mm) of a copper sample holder, covered by Mylar film (6  $\mu\text{m}$  thick) and frozen in liquid nitrogen. The samples were mounted into a Displex closed cycle He cryostat and their temperature maintained at 30 K to minimize radiation damage and thermal disorder.

#### 2.4.2. Data collection

X-ray absorption and fluorescence were collected at undulator beam line Sector 18 ID-D, the BioCAT facility in Advance Photon Source at Argonne National Laboratories, Argonne, IL. The beam is fed through double Si(III) crystal monochromator while harmonic rejection is attained by using a harmonic rejection mirror. Focused beam size was 100  $\mu\text{m}$  by 150  $\mu\text{m}$  with flux of 1014 photons/sec in 10–4 DE/E bandwidth. The incident X-ray beam intensity  $I_0$  was monitored by a  $N_2$  gas-filled ion chamber and X-ray fluorescence was monitored by the advanced multilayer detector. Fe  $\alpha K$ -edge was measured between X-ray energies of 7100 eV and 7500 eV. To minimize radiation damage 60 s scans were taken at each location on the samples of PSI core preparation at 30 K. After measurements no radiation burns were observed on the sample and P700 photooxidation in the PS I was similar to the activity measured prior to the exposure to X ray radiation.

#### 2.4.3. Data processing and analysis

The multiple X-ray fluorescence scans of a given sample were divided into two partial sums and a total sum, and averaged. The smooth atomic background was removed using the MacXAFS data analysis program which is based on the University of Washington program [31]. Data reduction consisted of edge determination at 7120 eV, deglitching, pre-edge background removal, edge normalization and post-edge background removal with cubic spline fit. The extraction of the EXAFS signal was followed by conversion of energy to

wave number  $k$ . Fourier transform was performed over the  $k$ -range  $k=3\text{--}12\text{ \AA}^{-1}$  of the  $k^3$ -weighted data with respect to  $k\chi(k)$  to obtain an atom distribution function with respect to the radial distance  $R$  around the central atom. The EXAFS contribution in real space of the two selected contributions was fitted by a single scattering formula, using the linearized least square procedure. For determination of the native structure a [4Fe–4S] model iron–sulfur cluster was extracted from the crystallographic coordinates of PS I (Protein Data Bank Code 1JB0). For determination of the C565S/D566E mutant  $F_X$ , the structure was modified by a Chem3D (Cambridge Scientific Computing) editor to include two oxygen atoms and the energy was minimized (details of the models are given in Section 3.3.2. and Fig. 4). This provided a chemically plausible starting structure, to calculate the Self Consistent Field (SCF) by using FEFF7/8 of Rehr et al. [32]. The calculated SCF was consequently used to determine the XAFS, and the sulfur and iron scattering of this model. A shift of 8 eV was applied to the XAFS to align the experimental and theoretical spectra and an  $S_0^2$  of 0.8 was assumed. A 4 eV shift was applied to account for differences between the nominal  $E_0$  (taken at the half of the edge step) of the experimental data, and the position of the energy zero calculated by FEFF8, which was 4 eV higher than the half edge step of the calculated FEFF8 XANES spectrum. An additional 4 eV shift was also found to give optimal fits, which is within the normal range of variation in fitting. The data of the native and the mutant were divided into three partial sums. The fluctuations observed in independent partial sums were taken as a measure of the noise level in the spectra. More than 30 fits were performed and the uncertainties associated with the errors in energy threshold and the amplitude reduction factor  $S_0^2$  were included.

### 3. Results

#### 3.1. XAS studies

The activity and the composition of all PsaC-deficient PS I samples used in XAS studies were determined before and after X-ray measurements. The subunit composition as determined by SDS-PAGE and Western blotting indicated that the preparations contained all subunits except for PsaC, D and E. The electron transfer activity was determined by measurement of the rate of P700<sup>+</sup> reduction following oxidation by single turnover flash. The results indicated that electrons were transferred from P700 to the quinone in PsaC-deficient PS I as was previously shown [16]. There was an approximately 15% loss of activity in the PsaC-deficient C565S/D566E mutant which was probably due to a damage caused to  $F_X$  during the isolation of PS I. However, isolation of PS I in the presence of Na<sub>2</sub>S reduced the extent of inactivation (see details of the kinetic studies in Section 3.4). There was less than 5% loss of activity after X-ray measurements. The structures of the native and the modified iron–sulfur cluster  $F_X$  in PsaC-deficient PS I were determined by X-ray absorption spectroscopy (XAS). Although a similar structure was determined by crystallography in PS I from *TS. elongatus* [3], it was difficult to obtain highly diffracting crystals from PS I prepared from the native and the mutant of *Synechocystis* sp. PCC 6803 [33]. However, after the removal of subunit PsaC that binds the iron–sulfur clusters  $F_{A/B}$ , the XAS of  $F_X$  could be measured in the core preparation without interference by the two other iron–sulfur clusters. The structure of  $F_X$  in the native and the mutant PS I was studied by X-ray absorption near edge structure (XANES) and by extended X-ray absorption fine structure (EXAFS) spectroscopy. EXAFS is a valuable technique for the elucidation of the structure of metal centers in proteins in general [34] and of iron centers in particular [34–36]. The technique measures the transition from the core electronic states of the metal to the excited electronic or continuum states. XAS can be conducted in any state of matter such as gas, liquid or solid phases. Spectral analysis near the electronic transition (XANES) provides information about the metal charge state and its geometry. Spectral analysis at energies above the absorption edge, in the EXAFS region,

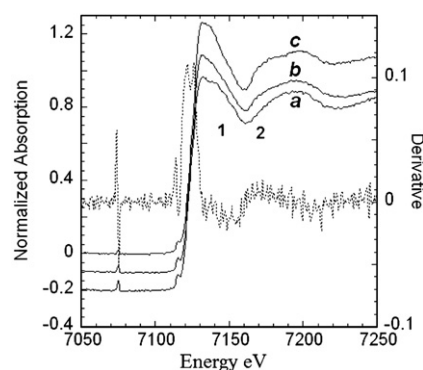


**Fig. 1.** X-ray absorption near-edge spectra (XANES) of the iron of the [4Fe–4S] iron–sulfur cluster  $F_X$  in PsaC-deficient PS I of the native and the C565S/D566E. The raw spectra of the iron in PsaC-deficient PS I from the native (a) and the C565S/D566E mutant isolated in the presence of Na<sub>2</sub>S (b) and C565S/D566E in the absence of Na<sub>2</sub>S (c) mutant are the sum of 300 scans taken at X-ray energies between 7050 and 7250 eV at 30 K. The derivatives indicate the absorption peaks, two of which are labeled (1) and (2).

provides structural information about the coordination numbers, and the types and distances of the neighboring atoms from the central absorbing atom. In addition, XAS is an effective tool for structural determination of the iron in the iron–sulfur cluster  $F_X$ , that has a weak spectroscopic signal in EPR and in visible absorption wavelengths.

#### 3.2. XANES measurements

The raw X-ray absorption spectra of the edge of the iron in the iron–sulfur cluster  $F_X$  in native PsaC-depleted PS I from *Synechocystis* (Fig. 1a) was similar to that observed in the urea-depleted PsaC core-protein of PS I from *Synechococcus* 6301 observed earlier [18]. One can observe, however substantial changes between the spectrum of the native and the C565S/D566E mutant  $F_X$  in PsaC-depleted PS I preparations from *Synechocystis* (Fig. 1a, c). The first derivative of the pre-edge and the first edge peaks have the same energies of 7113 eV and 7122 eV, but the steepness of the pre-edge is greater in the native than in that of the C565S/D566E mutant. Although the energies of the second edge peak at 7147 eV are the same, the native has a steeper peaks than the C565S/D566E mutant (Fig. 1a, c). The most significant changes in the XANES are seen in the peak (1) at derivative energy of 7149 eV of the native that is absent in the mutant and the appearance of the peak (2) at derivative energy of 7192 eV in the mutant that is absent in the native PS I. The differences between the native and the mutant were moderated when the PS I of the mutant was isolated in the presence of Na<sub>2</sub>S (Fig. 1b). However, the differences in peaks (1) and (2) between the native and the mutant remained (Fig. 1a, b). We relate these changes in peak intensity in the XANES to the replacement of one sulfur ligand of the iron–sulfur cluster by oxygen in the C565S/D566E mutant, the shortening of the Fe–O bond in comparison to the Fe–S bond, and the distortion of the symmetry of the cluster due to atom change and bond distance changes. It is possible that in the mutant the replacement of cysteine by serine was accompanied by the ligation of more than one oxygen atom to the iron (see EXAFS analysis). These in turn caused differences in the single and the multiple scattering patterns and resulted in apparent changes in the XANES.

#### 3.3. EXAFS analysis

The EXAFS data analyses of the PsaC-deficient PS I of the native and the C565S/D566E mutant were conducted in order to obtain more precise structural information. The normalized X-ray fluorescence spectra of the iron in the native C565S/D566E mutant isolated in the absence and in the presence of Na<sub>2</sub>S (Fig. 2.1) were used for EXAFS analysis. Standard and simultaneous curve-fitting procedures were

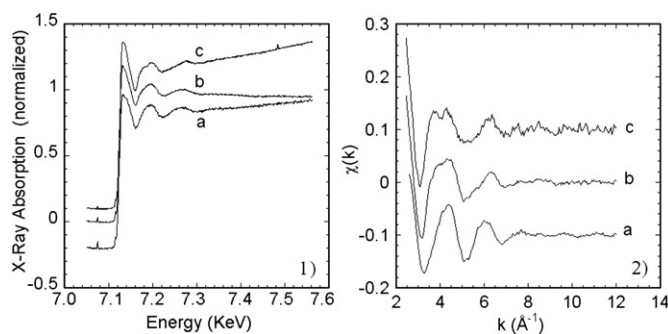


**Fig. 2.** X-ray absorption spectra of the iron of the [4Fe-4S] iron-sulfur cluster  $F_X$  in the PsaC-deficient PS I. The normalized spectra of the iron in PsaC-deficient PS I from the native (a) and the C565S/D566E mutant isolated in the presence of  $\text{Na}_2\text{S}$  (b) and C565S/D566E in the absence of  $\text{Na}_2\text{S}$  (c) are the sum of 300 60 s scans taken at X-ray energies between 7050 and 7560 eV at 30 K. The  $k$ -edge energy at 7127 eV. EXAFS data (1) were extracted following background removal. The  $k\chi(k)$  data (2) were calculated as a function of the photoelectron wave vector  $k$  ( $\text{\AA}^{-1}$ ) from the X-ray absorption spectra (1).

used to fit the FEFF7 and FEFF8 theoretical data [32] to the real and imaginary parts of the Fourier-transformed  $\chi(k)$ . The  $k^3$  or  $k^2$  weighting factor and the Hanning window function, defined between 3 and 12  $\text{\AA}^{-1}$  for native and 2 to 11  $\text{\AA}^{-1}$  for the mutant, were used in Fourier transforms. During fitting procedure, the corrections to the energy origin ( $\Delta E_0$ ), bond distances ( $\Delta R$ ), and mean square disorders of the distances ( $\sigma^2$ ) were varied until the best fit was obtained. The number of relevant independent data points  $N_{\text{ind}}$  in the data was calculated using the equation [31].

$$N_{\text{ind}} = \frac{2 \Delta k \Delta r}{\pi}$$

where  $\Delta k$  and  $\Delta r$  represent the data ranges in  $k$  and  $r$  spaces, respectively. The equation implies that the number of fit variables  $P$  should be smaller than  $N_{\text{ind}}$ . To reduce the number of fit variables, we fixed the many-body factor  $S_0^2$  at 0.8, and the following fitting procedures were developed.

### 3.3.1. Analysis of the structure of $F_X$ in the native PS I

The data of the native PsaC-depleted PS I were batched into two independent partial sums, and a total sum. Conventional methods of normalization, background subtraction and extraction of the EXAFS signal were applied. The  $k\chi(k)$  data were calculated as a function of the photoelectron wave vector  $k$  ( $\text{\AA}^{-1}$ ) from the X-ray absorption spectra (Fig. 2.2a). Fourier transform were performed over the  $k$ -range

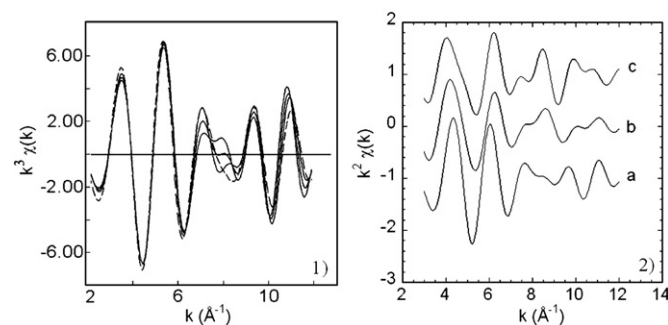


**Fig. 3.** The calculated back-transformed first two shells of the PsaC-deficient PS I. The  $k\chi(k)$  data (in Fig. 2.2) were  $k^3$ -weighted (1) for the native or  $k^2$ -weighted (2) for the native (a) and the C565S/D566E mutant isolated in the presence of  $\text{Na}_2\text{S}$  (b) and C565S/D566E in the absence of  $\text{Na}_2\text{S}$  (c) and Fourier transformed. Fit of the first two shells of the [4Fe-4S] model compound to the back-transformed measured data of the native PsaC-deficient PS I is shown (1). The two shells of the [4Fe-4S] model compound calculated by FEFF8 were fitted (...) to the total sum and to two partial sums of the first two shells of the measured data. Best fit values: Fe-S 4 S atoms,  $R=2.27 \text{ \AA}$ ,  $\sigma^2=0.007$  and Fe-Fe 3 Fe atoms,  $R=2.69 \text{ \AA}$  and  $\sigma^2=0.007$ .

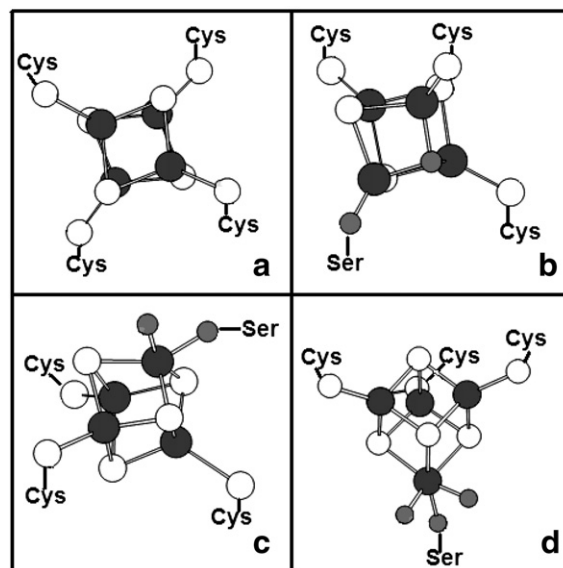


**Fig. 4.** Models of iron-sulfur clusters used for fitting of the experimental EXAFS data of the clusters in PS I. The wild-type cluster of a distorted tetrahedral [4Fe-4S] was taken from the crystalline structure of  $F_X$  in PS I (PDB code 1JB0). This cluster was also modified to substitute sulfur by oxygen, and to add oxygen atoms by the Chem3D graphic program. The structures were energy minimized. In the clusters each Fe atom (black) is bound on the average to 3 Fe and to 4 S (white), (a); 3 S and 1 O (gray) (b); 3.5 S and 0.5 O, (c); 3.5 S and 0.75 O (d). The average Fe-Fe distances are 2.67  $\text{\AA}$ , 2.93  $\text{\AA}$ , 2.69  $\text{\AA}$  and 2.69  $\text{\AA}$  in (a), (b), (c), and (d), respectively. The average Fe-S distances are 2.28  $\text{\AA}$ , 2.28  $\text{\AA}$ , 2.27  $\text{\AA}$  and 2.27  $\text{\AA}$  in (a), (b), (c) and (d), respectively. The average Fe-O distances are 1.84  $\text{\AA}$ , 1.81  $\text{\AA}$  and 1.83  $\text{\AA}$  in (b), (c) and (d), respectively. The amino acids Cys and Ser that serve as protein ligands for the clusters are indicated.

$k=3-12 \text{ \AA}^{-1}$ . The  $k\chi(k)$  of the data were  $k^3$ -weighted (Fig. 3.1) and Fourier transformed, and the first two shells were back-transformed (not shown). The fluctuations observed between independent partial sums were taken as a measure of the noise level in the spectra. The data set was sufficiently reproducible to permit reliable EXAFS data analysis. FEFF8 was used to generate imaginary and real part of the Fourier transform using the tetrahedral model similar to that in Fig. 4a. The model iron sulfur cluster was constructed in the CACHE molecule editor (Oxford Molecular) and the energy was minimized using molecular mechanics. This provided a chemically plausible starting structure, with Fe-S distance 2.20  $\text{\AA}$  and Fe-Fe 3.06  $\text{\AA}$ . Self consistent field (SCF) calculations were done using FEFF8 to calculate the XAFS, and the sulfur and iron scattering single scattering signals were calculated. A shift of 8 eV in the  $\Delta E_0$  was applied for fit of the theoretical to the real data and  $S_0^2$  of 0.8 was assumed. More than 30 fits were performed and uncertainties associated with errors in energy threshold and amplitude reduction factor  $S_0^2$  were included (Fig. 3.1). The best fit of the data on the native PS I was consistent with a 4Fe-4S ferredoxin-like cluster with an average 4 S atoms, Fe-S

**Table 1**

Structural parameters of the iron-sulfur cluster  $F_X$  of the native and the C565S/D566E mutant as obtained by EXAFS analysis

PS I	Ligand	Bond distance ( $\text{\AA}$ )	Atom number	$\sigma^2$
WT	Fe-S	$2.27 \pm 7^{-3}$	4	$7.0^{-3}$
	Fe-Fe	$2.69 \pm 7^{-3}$	3	$7.0^{-3}$
C565S/D566E	Fe-O	$1.81 \pm 4^{-3}$	1	$4.6^{-3}$
	Fe-S	$2.20 \pm 1^{-2}$	4	$1.2^{-2}$
	Fe-Fe	$2.60 \pm 5^{-2}$	3	$5.7^{-2}$

The data obtained from a fit of the first two shells of the [4Fe-4S] model compound (Fig. 4a and c) to the back-transformed  $k\chi(k)$ ,  $k^3$  or  $k^2$ -weighted measured data. The two shells of the [4Fe-4S] model compound calculated by FEFF7 program were fitted to the first two shells of the measured data of the PsaC-deficient PS I of the wild type (WT) and the C565S/D566E mutant.

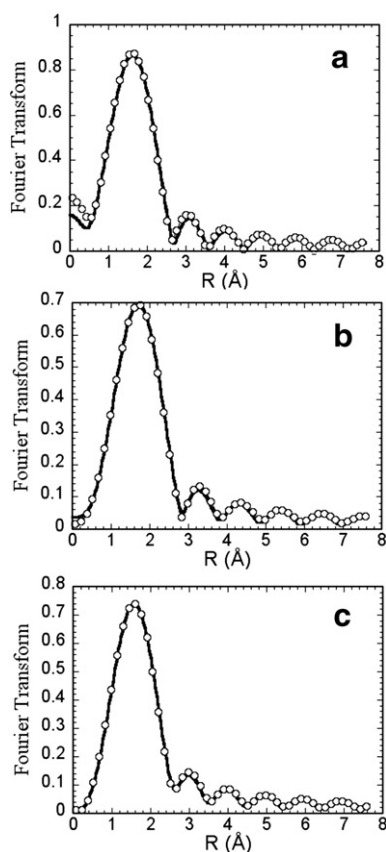


**Fig. 5.** FEFF fit of the calculated back-transformed first two shells of the PsaC-deficient PS I. Fit of the first two shells of the [4Fe–4S] models (Fig. 4a and c) to the back-transformed  $k\chi(k)$ ,  $k^2$ -weighted measured data. The two shells of the [4Fe–4S] models calculated by FEFF7 program were fitted to the first two shells of the measured data. Fourier transformed and the first two shells back-transformed data are presented in R space for PsaC-deficient PS I of the native (a), the C565S/D566E mutant isolated in the presence of Na<sub>2</sub>S (b) and C565S/D566E mutants (c).

$R=2.27$  Å,  $\sigma^2=0.007$  and for Fe–Fe 3 Fe atoms,  $R=2.69$  Å and  $\sigma^2=0.007$  (Table 1).

For comparison, a structure determination was also attempted by using the coordinates of iron–sulfur cluster from the crystallographic data of PS I as presented in the Protein Data Bank code 1JB0. These coordinates (see model Fig. 4a) were used as input data in the FEFF7 program to calculate the XAFS, and the sulfur and iron scattering singles. The  $k\chi(k)$  data were extracted from the XAFS measurements were  $k^2$ -weighted, Fourier transformed and best fitted to the theoretical first two shells of the EXAFS signal (Fig. 5a). The best fit of the data gave Fe–Fe of an average of 3 Fe atoms,  $R=2.62$  Å,  $\sigma^2=0.017$  and for Fe–S, 4 S atoms,  $R=2.27$  Å and  $\sigma^2=0.015$ . There was good agreement in the analyses used in the two methods of calculation and also with the previously published data [18].

### 3.3.2. Analysis of the structure of $F_X$ in the C565S/D566E mutant PS I

The XAS data of the C565S/D566E mutant PsaC-depleted PS I were analyzed essentially as for the wild type except that the  $k\chi(k)$  of the data were  $k^2$ -weighted (Fig. 3.2), and Fourier transformed over the  $k$ -range  $k=2$ – $11$  Å<sup>-1</sup>. Initial attempts to fit the data suggested that there was an average of approximately one oxygen atom per Fe, indicating that there was more than one oxygen atom at the first coordination shell of the iron in the cluster. This was surprising since only one of sulfur atoms in the cluster was expected to be replaced by oxygen as a result of the replacement of one of the cysteine ligands of the iron by serine. We therefore, generated models in which the iron in the cluster is ligated to more than one oxygen atoms (Fig. 4b–d) to be used as

input coordinate for the theoretical simulation of the EXAFS signal. For generation of the models, we modified the coordinates of the iron–sulfur cluster of PS I (PDB code 1JB0), by replacement of one of the cysteine sulfur ligands of the iron by oxygen from serine, and replacement of one additional sulfur in the cluster adjacent to this iron by a second oxygen (Fig. 4b). The model was built and energy minimized using Chem3D program. In other models, one of the cysteine sulfur ligands of the iron in the cluster was replaced by two and three oxygen atoms and the structure was energy minimized (Fig. 4c and d). The structure of the model in Fig. 4d resembles the structure of one of the irons in the iron–sulfur cluster of aconitase [37] that has three oxygen atoms in the first coordination shell.

The coordinates of the models (Fig. 4) were used as input data for the FEFF7 program for generation of the sulfur, oxygen and iron scattering singles. We could not obtain good fit when the coordinates of the model in which one atom of inorganic sulfur in the cluster was replaced by oxygen (Fig. 4b). Using the coordinates of the model in Fig. 4c, the best fit of the theoretical Fourier transform of the first two shells to the Fourier transformed  $k^2$ -weighted  $k\chi(k)$  data are shown in Fig. 5b. The results of best fit for first mixed shell were for Fe–O an average of 1 O atom,  $R=1.81$  Å,  $\sigma^2=0.0046$ ; for Fe–S were 3 S atoms,  $R=2.20$  Å,  $\sigma^2=0.012$  and second shell for Fe–Fe were 3 Fe atoms,  $R=2.60$  Å,  $\sigma^2=0.057$  (Table 1). A modified iron–sulfur cluster that can yield an average bond Fe–O of 1.81 Å for an average of one oxygen atom per iron atom and three sulfur per one iron atom, requires the replacement of one sulfur atom by oxygen and the addition of three more oxygen atoms at the first coordination shell of the iron. A model of a modified iron–sulfur cluster containing three oxygen atoms at the first shell of the iron is presented (Fig. 4d).

There were some differences between the XANES data of  $F_X$  in PS I from the C565S/D566E mutant isolated in the presence and the absence of Na<sub>2</sub>S. However, analysis of the EXAFS data gave similar results to those obtained from the PS I isolated in the absence of this reagent. The coordinates of the model (Fig. 4c) were used as input data for a FEFF7 program for generation of the sulfur, oxygen and iron scattering singles. The best fit of the theoretical Fourier transform of the first three shells to the Fourier transformed  $k^2$ -weighted  $k\chi(k)$  data are shown in Fig. 5c. The best fit for Fe–O in the first mixed shell were  $R=1.83$  Å, 1 O atom,  $\sigma^2=0.018$ ; for Fe–S in the first mixed shell were  $R=2.20$  Å, 3 S atoms,  $\sigma^2=0.011$ ; and for Fe–Fe in the second shell were  $R=2.53$  Å, 3 Fe atoms,  $\sigma^2=0.033$ . It can be assumed that the changes in the structure caused by the replacement of one of the cysteine ligands by serine induce the attachment of two or three water molecules to the iron in the iron–sulfur cluster. The additions of the oxygen atoms to the first shell of the iron could be monitored by XAS.

### 3.4. The effect of structural modification in the iron–sulfur cluster on electron transport in PS I from C565S/D566E mutant

The observed changes in the structure of the iron–sulfur cluster  $F_X$  might be used to explain the previously observed changes in electron transport in PS I isolated from C565S/D566E mutant [16]. The electron transport between the quinone and the iron sulfur cluster  $F_X$  was measured directly by observing the rate of oxidation of the photo reduced quinone. The oxidation of  $A_1^-$  measured at 380 nm occurred essentially with  $t_{1/2} \approx 3$  μs, i.e., more than one order of magnitude slower than in wild type PS I where a biphasic oxidation with  $t_{1/2}$  of 8.3 ns and 180 ns was measured [16]. We attributed the slow down in the rate of electron transfer to the addition of oxygen ligands to one of the irons in the iron–sulfur cluster, as determined by XAS.

Changes in the rate of electron transport were also indirectly measured by determination of the effect of the modification on the rate of the decay of flash-induced P700<sup>+</sup> in PS I from C565S/D566E mutant. In isolated PS I, photo-oxidized P700 is reduced either by the final electron acceptor or by the intermediate electron transport carriers. The rate of reduction depended on proximity of the reducing

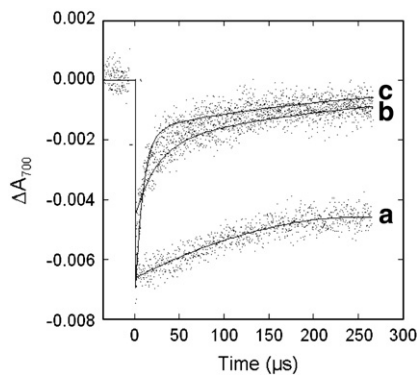


**Fig. 6.** Flash-induced transient oxidation of P700 in PS I complexes from the PsaC-deficient mutant. The absorption changes were measured at 700 nm in PS I complex of the C565S/D566E mutant (a), in the PsaC-deficient PS I of the native (b), and in the PsaC-deficient PS I of the C565S/D566E mutant isolated in the presence of Na<sub>2</sub>S (c). The fast decreases in absorption following a 10 ns laser flash were due to the rapid photooxidation of P700. PS I complexes were suspended at a Chl concentration of 60 μg/ml in 50 mM Tris-HCl, pH 8.3, containing 1.7 mM sodium ascorbate and 33 μM DCIP, 22 °C.

carrier to P700<sup>+</sup> and the redox potential differences. The slow-down in the forward electron transfer between the quinone was expressed also as a small change in the rate of reduction of photo-oxidized P700. About 85% of the total amplitude decayed with virtually the same kinetics in the 20 ms to 80 ms range as in wild type PS I, indicating that forward electron transfer to F<sub>A/B</sub> occurred in the large majority of C565S/D566E mutant PS I. Only 15% of the total amplitude decayed in 3 μs to 20 μs (Fig. 6a) [16], a time range typical for charge recombination between A<sub>1</sub> and P700<sup>+</sup> [38]. Structural determination of F<sub>X</sub> was done not on isolated PS I but on the PsaC-deficient PS I, a core preparation, which lacked subunits PsaC, PsaD and PsaE due to genetic disruption of the *psaC* gene. On removal of PsaC subunit containing iron-sulfur clusters F<sub>A</sub> and F<sub>B</sub> from PS I, it was expected that P700<sup>+</sup> would be reduced by F<sub>X</sub>. Yet the rate of reduction of P700<sup>+</sup> measured as absorption change at 700 nm was much faster in the native PsaC-depleted PS I (Fig. 6b) with  $t_{1/2}$  = 7–43 μs (66% of the total absorption change) for the main component and  $t_{1/2}$  = 0.2–100 ms (33%) compared to only 15% of the total amplitude decayed in 3 μs to 20 μs (Fig. 6a). The fast μs time scale reduction rates of P700<sup>+</sup> were assigned to A<sub>1</sub>/P700<sup>+</sup> recombination and slow ms time scale rates were related to charge recombination between P700<sup>+</sup> and F<sub>X</sub>. The results of the kinetic measurements of the preparations used for XAS determination in this work were in agreement with our previous measurements of similar PS I complexes in which P700 changes were measured at 820 nm [16]. The rate of P700<sup>+</sup> reduction in PsaC-deficient PS I of the mutant C565S/D566E had a main kinetic component with  $t_{1/2}$  = 7–45 μs (86%) and a minor component with  $t_{1/2}$  = 0.7–24 ms (14%). We have suggested previously that the inhibition of electron transport to F<sub>X</sub> was caused by the change in Coulomb interactions upon removal of the extrinsic subunits, and not by the damage to F<sub>X</sub>. We observed that the removal of subunits PsaC, PsaD and PsaE results breaking six salt bridges between these subunits and PsaB and PsaA. Taking into account the distances between F<sub>X</sub> and the six surface charges, their cumulated potential in the center of F<sub>X</sub> was -68 mV [16].

In order to determine whether F<sub>X</sub> was damaged in the PsaC-deficient PS I, we attempted to reconstitute the iron-sulfur cluster. The reconstitution was carried out in the presence of β-mercaptoethanol, Fe<sup>3+</sup> and S<sup>2-</sup> or in the presence of β-mercaptoethanol alone. It was only in the PsaC-deficient PS I of the mutant C565S/D566E that the reconstitution increased the extent of the P700<sup>+</sup> reduction phase with  $t_{1/2}$  = 0.7–27 ms up to 15% of the total absorption change. Treatment of PsaC-deficient PS I of the native did not change the kinetics of P700<sup>+</sup> reduction. These results suggest that only in the PsaC-deficient PS I from the mutant C565S/D566E were some of F<sub>X</sub> centers were

degraded. The rate of P700<sup>+</sup> reduction of the PsaC-deficient PS I from the C565S/D566E isolated in the presence of Na<sub>2</sub>S had a minor component with  $t_{1/2}$  = 0.7–27 ms (15%) (Fig. 6c), and was essentially similar to the rate in the PsaC-deficient PS I of the native (Fig. 6b). To protect the mutant PS I from suspected oxidation damage that might have occurred during isolation of the complex, we included Na<sub>2</sub>S in the isolation medium of the membranes and the protein. However, only slight differences could be detected in the structure of the modified F<sub>X</sub> prepared by the two methods.

## 4. Discussion

### 4.1. Structure of the native iron-sulfur cluster F<sub>X</sub> in PS I

For determination of the structure of F<sub>X</sub> in the native PsaC-depleted PS I, we used two models. In one we used the coordinates of the iron-sulfur cluster (Fig. 4a) obtained by crystallographic determination of PS I (PDB code 1JB0). In the other we used the coordinates of a theoretically constructed cubic [4Fe-4S] iron-sulfur cluster similar to the model in Fig. 4a. The results were in agreement with the structure obtained by crystallography of PS I from *TS. elongatus* [3] and by EXAFS analysis of core protein preparation of PS I from *Synechococcus* 6301 [18]. The results confirmed that the PsaC-depleted PS I preparation contained an intact iron-sulfur cluster and that the measurement and the analytical method used in the present experiments were reliable.

### 4.2. Structure of the modified iron-sulfur cluster F<sub>X</sub> in the C565S/D566E mutant

Initial data fit suggested that there was more than one oxygen atom at the first coordination shell of the iron in the cluster. To generate models in which the iron in the cluster is ligated to more than one oxygen atom (Fig. 4c, d) we modified the coordinates of the iron-sulfur cluster of PS I (PDB code 1JB0). To obtain the model in Fig. 4b, we replaced one of the cysteine sulfur ligands of the iron by oxygen from serine and replaced one additional sulfur in the cluster adjacent to this iron by a second oxygen atom (Fig. 4b). Energy minimization using Chem3D was applied. In the cluster each Fe atom was bound on the average to 3Fe, 3S and 1O. The average Fe-Fe distance was 2.93 Å and the average Fe-S distance was 2.28 Å. The experimental data could not be well fitted to the theoretical data using this model because of the rather large Fe-Fe distance and the large disparity in distance between the various irons. These results were not unpredictable because, although such a structure could be assumed, to our knowledge there are neither natural nor synthetic iron-sulfur clusters that contain a single oxygen in place of one of the inorganic sulfurs in the cluster.

In a second refined model, one of the cysteine sulfur ligand of the iron in the cluster was replaced by two oxygen atoms and the energy of the structure minimized (Fig. 4c). Although only one water molecule was observed in the crystal structure of PS I at 2.5 Å resolution near the iron-sulfur cluster F<sub>X</sub>, it is possible that there are several non-resolved water molecules. Upon replacement of cysteine by serine in the mutant there was a shortening of the distance between the iron and the ligating atom. These structural and polarity changes could have caused direct attachment of water hydroxyls to the iron in the cluster. Alternatively, the removal of the subunits could have exposed the F<sub>X</sub> to additional solvent water molecules. However, if that were the case one would expect to find more oxygen atoms in near the iron of F<sub>X</sub> also in the native PsaC-deficient PS I.

The third model in which one of the cysteine sulfur ligand of the iron in the cluster was replaced by three oxygen atoms is shown in Fig. 4d. The proposed structure resembles the structure of one of the irons in the iron-sulfur cluster of aconitase [37] that has three oxygen atoms in the first coordination shell. In the cluster each Fe atom is bound to 3

Fe, 3.75 S and 0.75 O. The average Fe–Fe distance is 2.69 Å, the average Fe–S distances are 2.27 Å and the average Fe–O distances are 1.8 Å and 1.83 Å (Fig. 5d). Using the coordinates from the model in Fig. 4c as input data, we could obtain a good fit with the experimental EXAFS data. The results indicate that the modified  $F_X$  is a distorted cubic iron–sulfur cluster in which one of the irons in the cluster is attached to three oxygen atoms, one donated by the serine hydroxyl while two more from water molecules in the protein. The average Fe–O distance is 1.81 Å while the average Fe–Fe distance is 2.60 Å and the average Fe–S distance is 2.20 Å. These results are in harmony with the observed shortening of the Fe–O distance by 0.11 Å–0.4 Å in comparison to the Fe–S distance upon changing cysteine to serine in iron–sulfur cluster proteins [39–41].

#### 4.3. XANES measurements

Qualitative evaluation of the differences in the XANES of the native and the mutant PS I support the results obtained from EXAFS analysis. The raw X-ray absorption spectra of the edge of the iron in the iron–sulfur cluster  $F_X$  in native PsaC-depleted PS I from *Synechocystis* was similar to that observed in urea-depleted PsaC core-protein of PS I from *Synechococcus* 6301 [18]. However there are substantial changes between the spectrum of the native and the C565S/D566E mutant  $F_X$  in PsaC-depleted PS I preparations from *Synechocystis*. The most striking changes in the XANES were seen in peak (1) at energy of 7149 eV of the native that is absent in the mutant, and the appearance of peak (2) at energy of 7192 eV in the mutant that is absent in the native PS I. The differences between the native and the mutant were however moderated when the PS I of the mutant was isolated in the presence of  $Na_2S$ . These changes in peak intensity in the XANES may result from the replacement of one sulfur ligand of the iron–sulfur cluster by oxygen in the C565S/D566E mutant, the shortening of the Fe–O bond in comparison to the Fe–S bond and the distortion of the symmetry of the cluster due to atom change and bond distance changes. Similar changes in XANES were also observed in serine mutant of rubredoxin [41].

#### 4.4. Structure–function studies of intra-subunit interactions in the environment of the iron–sulfur cluster $F_X$

The iron–sulfur cluster  $F_X$  is located on the core subunits PsaA/B at the interphase with subunit PsaC in PS I. It is the last carrier of the primary section of the electron transfer chain.  $F_X$  mediates electrons across the subunit interphase to the terminal carriers  $F_{A/B}$  on subunit PsaC. We have previously suggested [16] that this strategic location  $F_X$  facilitates a potential role of the carrier as a control switch of electron transfer in PS I. For such a role, the carrier should be able to affect the electron transport in response to changes in the environment. Indeed, there are numerous findings that indicate that the electron transfer to  $F_X$  is changed in response to the state of the surroundings. The rate is sensitive to the redox state of  $F_{A/B}$ , to the presence of these iron–sulfur clusters, to temperature, and to inter- and intra-subunit interactions. All these responses are indicative of a potential role of controlling the electron flow in PS I. In this work we evaluated the structure–function relations of intra-subunit interactions by determination of the structure of the iron–sulfur cluster that has been modified by site-directed mutations using XAS. Two types of structural effects were identified. First, the deletion of subunit PsaC, which was done in order to remove the interference of iron–sulfur clusters  $F_{A/B}$  with the structural determination of  $F_X$ , resulted in strong inhibition of the electron transport to  $F_X$ . The reason for such change had been traced earlier to the change in the Coulomb effect due to changes in subunit interactions [16]. The removal of PsaC subunit did not damage  $F_X$  since reconstitution of the iron–sulfur cluster did not change the rate of electron transport.  $F_X$  in the PsaC-depleted preparation was also found to be potentially functional, as a reconstitution of PS I by the addition

of subunits PsaC, PsaD and PsaE and of the iron–sulfur clusters recovered electron transport to  $F_{A/B}$  [16]. The second effect was the 20 fold decrease in the rate of electron transfer from the quinone to  $F_X$  as a result of a change of one of the cysteine ligand of the iron to serine. The structural basis for this effect was solved using XAS studies. The resolution of this effect has implications for understanding the factors that contribute to the very low potential of this iron–sulfur cluster.

#### 4.5. The effect of structural changes on electron transport

Structural determination indicated that in the modified cluster one of the irons was ligated to three oxygen atoms that had replaced a single cysteine sulfur atom. There is a need to evaluate the possible origins for the expected modification in electron transfer from  $A_1$  to  $F_X$  that resulted from this change.

According to non-adiabatic electron transfer theory [42], the electron transfer rate  $k_{et}$  is proportional to the square of electronic coupling ( $T_{DA}$ ) between electron donor and acceptor, and to the Franck–Condon factor (F.C.):

$$k_{et} = \frac{2\pi}{\hbar} |T_{DA}|^2 (\text{F.C.}) \quad (1)$$

$T_{DA}$  is not expected to change upon site-directed mutation, unless this replacement of amino acids would cause structural changes in the remaining PS I core complex that would modify the distance between  $A_1$  and  $F_X$ . The Franck–Condon factor can be expressed in a classical treatment of nuclear motion [42] as

$$(\text{F.C.}) = \frac{1}{\sqrt{4\pi\lambda k_B T} \exp\left[-\frac{(\Delta G^\circ + \lambda)^2}{4\lambda k_B T}\right]} \quad (2)$$

where  $k_B$  is the Boltzmann constant,  $T$  the absolute temperature,  $\Delta G^\circ$  the standard free energy change of the electron transfer reaction, and  $\lambda$  the reorganization energy. Replacement of one of the cysteine ligands of the cluster by serine could affect  $\Delta G^\circ$  and hence the electron transfer rate in two ways.

Replacing the cysteine sulfur ligand of the iron in the cluster by oxygen atoms should facilitate charge accumulation on  $F_X$  (from two to three negative charges upon reduction) and hence decrease  $\Delta G^\circ$ . Indeed, replacement of cysteine by serine in iron–sulfur clusters of ferredoxin and rubredoxin resulted in a more positive redox potential [39,41], although in Anabaena ferredoxin of the two cysteine ligand changes C46S and C49S, only the latter caused a +55 mV change in the redox potential [40]. According to Eqs. (1) and (2), decreasing  $\Delta G^\circ$  should increase the rate of electron transfer from  $A_1$  to  $F_X$  (the opposite case would only occur in the “inverted region” ( $-\Delta G^\circ > \lambda$ ) that can be safely excluded for this electron transfer [17]). However, we obtained a decrease in the rate of electron transfer in the C565S/D566E mutant.

The reorganization energy  $\lambda$  generally increases with increasing static dielectric constant of the environment of electron donor and acceptor [42]. Hence, we expect an increase of  $\lambda$  upon replacing hydrogen-bonded water molecules in the environment of the cluster by directly binding their oxygen atoms to the iron in the cluster. As  $|\Delta G^\circ| < \lambda$  for electron transfer from  $A_1$  to  $F_X$  [42], increasing  $\lambda$  should decrease the rate of this electron transfer (see Eq. (2)). The observed decrease in the rate of electron transfer would indicate that the change in reorganization energy had a greater effect than the change in  $|\Delta G^\circ|$  in the C565S/D566E mutant. Another possibility is that, unlike the Anabaena ferredoxin, there was no change in the redox potential of  $F_X$  due to the cysteine to serine change, and the decrease in electron transfer rate was only due to a change in the reorganization energy.

## Acknowledgements

Thanks to Dr. M. Paddock from UC San Diego for his help in editing the manuscript.

## References

- [1] P.R. Chitnis, N. Nelson, Photosystem I, in: L. Bogoras, I.K. Vasil (Eds.), *Photosynthetic Apparatus: Molecular Biology and Operation*, Academic Press, N.Y., 1991, pp. 177–224.
- [2] J.H. Golbeck, The binding of cofactors to photosystem I analyzed by spectroscopic and mutagenic methods, *Annu. Rev. Biophys. Biomol. Struct.* (2003) 236–237.
- [3] P. Jordan, P. Fromme, H.T. Witt, O. Klukas, W. Saenger, N. Krauss, Three-dimensional structure of cyanobacterial photosystem I at 2.5 Å resolution, *Nature* 411 (2001) 909–917.
- [4] A. Amunts, O. Drory, N. Nelson, The structure of a plant photosystem I supercomplex at 3.4 angstrom resolution, *Nature* 447 (2007) 58–63.
- [5] L.E. Fish, L. Bogorad, Identification and analysis of the maize P700 chlorophyll a apoproteins PSI-A1 and PSI-A2 by high pressure liquid chromatography analysis and partial sequence determination, *J. Biol. Chem.* 261 (1986) 8134–8139.
- [6] M.C.W. Evans, S.G. Reeves, R. Cammack, Determination of the oxidation–reduction potential of the bound iron–sulfur proteins of the primary electron acceptor complex of photosystem I in spinach chloroplasts, *FEBS Lett.* 49 (1974) 111–114.
- [7] P. Setif, H. Bottin, Identification of electron-transfer reactions involving the acceptor A1 of photosystem I at room temperature, *Biochemistry* 28 (1989) 2689–2697.
- [8] M.C.W. Evans, P. Heathcote, Effect of glycerol on the redox properties of the electron acceptor complex in spinach photosystem I particles, *Biochim. Biophys. Acta* 590 (1980) 89–96.
- [9] J. Luneberg, P. Fromme, P. Jekow, E. Schlodder, Spectroscopic characterization of PS I core complexes from thermophilic *Synechococcus* sp. Identical reoxidation kinetics of A1- before and after removal of the iron–sulfur-clusters FA and FB, *FEBS Lett.* 338 (1994) 197–202.
- [10] A. van der Est, C. Bock, J.H. Golbeck, K. Brettel, P. Setif, D. Stehlik, Electron transfer from the acceptor A1 to the iron–sulfur centers in photosystem I as studied by transient EPR spectroscopy, *Biochemistry* 33 (1994) 11789–11797.
- [11] P. Moenne-Loccoz, P. Heathcote, D.J. MacLachlan, M.C. Berry, I.H. Davis, M.C.W. Evans, Path of electron transfer in photosystem I: direct evidence of forward electron transfer from A1 to Fe–Sx, *Biochemistry* 33 (1994) 10037–10042.
- [12] P. Setif, K. Brettel, Forward electron transfer from phyloquinone A1 to iron–sulfur centers in spinach photosystem I, *Biochemistry* 32 (1993) 7846–7854.
- [13] E. Schlodder, K. Falkenberg, M. Gergeleit, K. Brettel, Temperature dependence of forward and reverse electron transfer from A1-, the reduced secondary electron acceptor in photosystem, *Biochemistry* 37 (1998) 9466–9476.
- [14] M. Guergova-Kuras, B. Boudreaux, A. Joliot, P. Joliot, K. Redding, Evidence for two active branches for electron transfer in photosystem I, *Proc. Natl. Acad. Sci. U. S. A.* 98 (2001) 4437–4442.
- [15] P. Joliot, A. Joliot, In vivo analysis of the electron transfer within photosystem I: are the two phyloquinones involved? *Biochemistry* 38 (1999) 11130–11136.
- [16] X.M. Gong, R. Agalarov, K. Brettel, C. Carmeli, Control of electron transport in photosystem I by the iron–sulfur cluster F–X in response to intra- and intersubunit interactions, *J. Biol. Chem.* 278 (2003) 19141–19150.
- [17] K. Brettel, Electron transfer and arrangement of the redox cofactors in Photosystem I, *Biochim. Biophys. Acta* 1318 (1997) 322–373.
- [18] A.E. McDermott, V.K. Yachandra, R.D. Guiles, K. Sauer, M.P. Klein, K.G. Parrett, J.H. Golbeck, EXAFS structural study of FX, the low-potential Fe–S center in photosystem I, *Biochemistry* 28 (1989) 8056–8059.
- [19] P.V. Warren, L.B. Smart, L. McIntosh, J.H. Golbeck, Site-directed conversion of cysteine-565 to serine in PsaB of photosystem I results in the assembly of [3Fe–4S] and [4Fe–4S] clusters in Fx. A mixed-ligand [4Fe–4S] cluster is capable of electron transfer to FA and FB, *Biochemistry* 32 (1993) 4411–4419.
- [20] I.R. Vassiliev, Y.S. Jung, L.B. Smart, R. Schulz, L. McIntosh, J.H. Golbeck, A mixed-ligand iron–sulfur cluster (C556SPaB or C565SPsaB) in the Fx-binding site leads to a decreased quantum efficiency of electron transfer in photosystem I, *Biophys. J.* 69 (1995) 1544–1553.
- [21] R. Rippka, J. Deruelles, J.B. Waterbury, M. Herdman, R.Y. Stanier, Generic assignments, strain histories and properties of pure cultures of cyanobacteria, *J. Gen. Microbiol.* 111 (1979) 1–16.
- [22] L.B. Smart, P.V. Warren, J.H. Golbeck, L. McIntosh, Mutational analysis of the structure and biogenesis of the photosystem I reaction center in the cyanobacterium *Synechocystis* sp PCC 6803, *Proc. Natl. Acad. Sci. U. S. A.* 90 (1993) 1132–1136.
- [23] M. Zeng, I. Sagi, M.C.W. Evans, N. Nelson, C. Carmeli, Site directed and suppressor mutations of Fx ligands in PsaB of photosystem I in *Synechocystis* sp PCC 6803, in: G. Gabar, J. Puszta (Eds.), *Photosynthesis: Mechanisms and Effects*, Kluwer Academic Publishers, Dordrecht, 1999, pp. 643–646.
- [24] S.L. Anderson, L. McIntosh, Light-activated heterotrophic growth of the cyanobacterium *Synechocystis* sp. strain PCC 6803: a blue-light-requiring process, *J. Bacteriol.* 173 (1991) 2761–2767.
- [25] U.K. Laemmli, Cleavage of structural proteins during the assembly of the head of bacteriophage T4, *Nature* 227 (1970) 680–685.
- [26] K.R. Tindall, T.A. Kunkel, Fidelity of DNA synthesis by the *Thermus aquaticus* DNA polymerase, *Biochemistry* 27 (1988) 6008–6013.
- [27] O.H. Lowry, N.L. Rosenbrough, A.L. Farr, R.J. Randall, Protein measurement with the folin phenol reagent, *J. Biol. Chem.* 193 (1951) 265–275.
- [28] D.I. Arnon, Copper enzymes in isolated chloroplasts. Polyphenoloxidase in beta vulgaris, *Plant Physiol.* 24 (1949) 1–15.
- [29] T. Hiyama, B. Ke, Difference spectra and extinction coefficients of P700, *Biochim. Biophys. Acta* 257 (1978) 160–171.
- [30] M.T. Zeng, X.M. Gong, M.C. Evans, N. Nelson, C. Carmeli, Stabilization of iron–sulfur cluster F(X) by intra-subunit interactions unraveled by suppressor and second site-directed mutations in PsaB of Photosystem I, *Biochim. Biophys. Acta* 1556 (2002) 254–264.
- [31] E.A. Stern, M. Newville, B. Ravel, Y. Yacoby, D. Haskel, The Uwxafs analysis package – philosophy and details, *Physica B* 209 (1995) 117–120.
- [32] J.J. Rehr, J. Muster de Leon, S.I. Zabinsky, R.C. Albers, Theoretical X-ray absorption fine structure standards, *J. Am. Chem. Soc.* 113 (1991) 5135–5140.
- [33] X.M. Gong, Genetic Approach to Intrasubunit Interactions in the Environment of the Iron–sulfur Cluster in Photosystem I from *Synechocystis* sp. PCC 6803, Tel Aviv University, 2002.
- [34] I. Sagi, G. Bunker, Y. Hochman, C. Carmeli, M.T. Zeng, Detection by X-ray absorption of the redox induced structural change in iron–sulfur cluster Fx in photosystem I, *Acta Phys. Polonica A* 91 (1997) 871–875.
- [35] K. Zhang, B. Chance, K.S. Reddy, I. Ayene, E.A. Stern, G. Bunker, Structural differences in solution and crystalline forms of met-myoglobin, *Biochemistry* 30 (1991) 9116–9120.
- [36] E. Krahn, B.J.R. Weiss, M. Krockel, J. Groppe, G. Henkel, S.P. Cramer, A.X. Trautwein, K. Schneider, A. Muller, The Fe-only nitrogenase from *Rhodospirillum rubrum*: identification of the cofactor, an unusual, high-nuclearity iron–sulfur cluster, by FeK-edge EXAFS and Fe-57 Mossbauer spectroscopy, *J. Biol. Inorg. Chem.* 7 (2002) 37–45.
- [37] S.J. Lloyd, H. Lauble, G.S. Prasad, C.D. Stout, The mechanism of aconitase: 1.8 Å resolution crystal structure of the S642a: citrate complex, *Protein Sci.* 8 (1999) 2655–2662.
- [38] K. Brettel, J.H. Golbeck, Spectral and kinetic characterization of electron acceptor A1 in a photosystem I core devoid of iron–sulfur centers FX, FB and FA, *Photosyn. Res.* 45 (1995) 183–193.
- [39] A.T. Kowal, M.T. Werth, A. Manodori, G. Cecchini, I. Schroder, R.P. Gunsalus, M.K. Johnson, Effect of cysteine to serine mutations on the properties of the [4Fe–4S] center in *Escherichia coli* fumarate reductase, *Biochemistry* 34 (1995) 12284–12293.
- [40] J.K. Hurley, A.M. Weber-Main, A.E. Hodges, M.T. Stankovich, M.M. Benning, H.M. Holden, H. Cheng, B. Xia, J.L. Markley, C. Genzor, C. Gomez-Moreno, R. Hafezi, G. Tollin, Iron–sulfur cluster cysteine-to-serine mutants of *Anabaena* [2Fe–2S] ferredoxin exhibit unexpected redox properties and are competent in electron transfer to Ferredoxin:NADP+ reductase, *Biochemistry* 36 (1997) 15109–15117.
- [41] Z. Xiao, M.J. Lavery, M.S. Ayhan, D.B. Scrofani, M.C.J. Wilce, J.M. Guss, P.A. Tregloan, G.N. George, A.G. Wedd, The Rubredoxin from *Clostridium pasteurianum*: mutation of the iron cysteinyl ligands to serine. Crystal and molecular structures of oxidized and dithionite-treated forms of the Cys42Ser mutant, *J. Am. Chem. Soc.* 120 (1998) 4135–4150.
- [42] R.A. Marcus, N. Sutin, Electron transfer in chemistry and biology, *Biochim. Biophys. Acta* 811 (1985) 265–322.